

Mechanism of substrate specificity in 5'-methylthioadenosine/S-adenosylhomocysteine nucleosidases

Karen K.W. Siu^{a,b}, Kyle Asmus^d, Allison N. Zhang^b, Cathy Horvatin^a, Sheng Li^d, Tong Liu^d, Barbara Moffatt^c, Virgil L. Woods Jr.^{d,*}, and P. Lynne Howell^{a,b,**}

^a Program in Molecular Structure and Function, Research Institute, The Hospital for Sick Children, 555 University Avenue, Toronto, Ontario, Canada M5G 1X8

^b Department of Biochemistry, Faculty of Medicine, University of Toronto, Medical Sciences Building, Toronto, Ontario, Canada M5S 1A8

^c Department of Biology, University of Waterloo, Waterloo, Ontario, Canada N2L 3G1

^d Department of Medicine and Biomedical Sciences, University of California, San Diego, La Jolla, CA 92093-0656, United States

Abstract

5'-Methylthioadenosine/S-adenosylhomocysteine (MTA/SAH) nucleosidase (MTAN) plays a key role in the methionine-recycling pathway of bacteria and plants. Despite extensive structural and biochemical studies, the molecular mechanism of substrate specificity for MTAN remains an outstanding question. Bacterial MTANs show comparable efficiency in hydrolyzing MTA and SAH, while the plant enzymes select preferentially for MTA, with either no or significantly reduced activity towards SAH. Bacterial and plant MTANs show significant conservation in the overall structure, and the adenine- and ribose-binding sites. The observation of a more constricted 5'-alkylthio binding site in *Arabidopsis thaliana* A α M-TAN1 and A α MTAN2, two plant MTAN homologues, led to the hypothesis that steric hindrance may play a role in substrate selection in plant MTANs. We show using isothermal titration calorimetry that SAH binds to both *Escherichia coli* MTAN (EcMTAN) and A α MTAN1 with comparable micromolar affinity. To understand why A α MTAN1 can bind but not hydrolyze SAH, we determined the structure of the protein–SAH complex at 2.2 Å resolution. The lack of catalytic activity appears to be related to the enzyme's inability to bind the substrate in a catalytically competent manner. The role of dynamics in substrate selection was also examined by probing the amide proton exchange rates of EcMTAN and A α MTAN1 *via* deuterium–hydrogen exchange coupled mass spectrometry. These results correlate with the B factors of available structures and the thermodynamic parameters associated with substrate binding, and suggest a higher level of conformational flexibility in the active site of EcMTAN. Our results implicate dynamics as an important factor in substrate selection in MTAN.

Keywords

5'-Methylthioadenosine/S-adenosylhomocysteine nucleosidase; Dynamics; Substrate specificity; Deuterium–hydrogen exchange coupled; mass spectrometry; Isothermal titration calorimetry

*Corresponding author. vwoods@ucsd.edu (V.L. Woods). **Corresponding author. howell@sickkids.ca (P.L. Howell).

1. Introduction

5'-Methylthioadenosine/S-adenosylhomocysteine nucleosidase (MTAN) plays an essential role in multiple metabolic pathways in bacteria and plants. In bacteria, MTAN is dual-substrate specific and is responsible for the hydrolysis of 5'-methylthioadenosine (MTA) and S-adenosylhomocysteine (SAH) to adenine and their corresponding thioriboses (Fig. 1) (Cornell et al., 1996; Singh et al., 2006; Della Ragione et al., 1985). Hydrolysis of MTA is a key step in the recycling pathway of methionine, an essential amino acid that is energetically expensive to synthesize (Sufrin et al., 1995; Riscoe et al., 1989). Accumulation of MTA also leads to negative feedback inhibition of polyamine biosynthesis (Pajula and Raina, 1979; Raina et al., 1982) and biological methylation (Borchardt et al., 1986). Efficient functioning of MTAN is also important for quorum sensing because the metabolic product of SAH hydrolysis, S-ribosylhomocysteine, serves as a substrate for the production of autoinducer-2, which has been implicated in intra- and interspecies communication (Schauder et al., 2001; Chen et al., 2002).

In plants, the methionine-recycling pathway is conjugated to the synthesis of ethylene, nicotianamine and phytosiderophores, which release MTA as a byproduct of the reactions (Burstenbinder et al., 2007; Baur and Yang, 1972; Roje, 2006). Plant MTANs play a dual role of preventing the accumulation of inhibitory MTA and ensuring efficient salvage of the nucleoside to methionine so that high levels of S-adenosylmethionine are available for ethylene synthesis (Guranowski et al., 1981). In plant species that produce high levels of ethylene, such as those that are submerged for prolonged periods or that have seasonal fruit ripening, MTAN is thought to be important in seed germination and fruit ripening. Nicotianamine shows high affinity for iron and other transition metals and is important in binding and trafficking these minerals in plants. In graminaceous plants, nicotianamine also serves as a substrate to produce phytosiderophores, which play a key role in iron absorption and transportation (Roje, 2006).

Unlike bacterial MTANs, the plant enzymes appear to be highly specific for MTA. Many plant MTAN homologues are unable to metabolize SAH and those that do show 84–87% reduction in activity relative to the hydrolysis of MTA (Guranowski et al., 1981; Rzewuski et al., 2007; Baxter and Coscia, 1973). Kinetic characterization of the two MTAN homologues found in the thale cress plant, *Arabidopsis thaliana*, showed that *At*MTAN1 is completely inactive towards SAH while *At*MTAN2 has 14% activity towards this substrate (Siu et al., 2008a). Structural comparison of *At*MTAN1 with the bacterial MTAN homologue from *Escherichia coli* (*Ec*M-TAN) showed significant conservation in the overall structure (Siu et al., 2008a). Close examination of the active sites suggested that the active site of *Ec*MTAN may be more disordered than that of *At*MTAN1 (Siu et al., 2008a). This observation was based on the absence of electron density for four active site residues and higher overall B factors for all active site residues of *Ec*MTAN. Also, when structures that represent the apo 'open' conformation of *Ec*MTAN (PDB code: 1JYS) and *At*MTAN1 (PDB code: 2QSU) were superimposed with the structures representing the 'closed' ligand-bound form (PDB codes: 1NC1 for *Ec*MTAN; 2QTG for *At*M-TAN1), more dramatic structural changes were identified in the bacterial enzyme (Siu et al., 2008a). These findings led to the hypothesis

that reduced conformational plasticity in the plant MTAN active site may contribute to its inability to bind SAH (Siu et al., 2008a; Park et al., 2009). To better understand the role that conformational flexibility may play in determining the substrate specificity of plant MTANs, we have examined the conformational dynamics of *Ec*MTAN and *At*MTAN1 using deuterium–hydrogen exchange coupled mass spectrometry (DXMS) and isothermal titration calorimetry (ITC). Our results represent the first direct study of dynamics in MTAN and rectify the previous misconception that some plant MTANs are inactive towards SAH because they are unable to bind the substrate. The crystal structure of *At*MTAN1 in complex with SAH was determined to 2.2 Å resolution. Comparison of this structure with the available substrate-analogue bound form of *At*MTAN1 (PDB: 2QTG) provides new insight into the lack of SAH activity in this enzyme.

2. Materials and methods

2.1. Preparation of *Ec*MTAN and *At*MTAN1

*Ec*MTAN and *At*MTAN1 were overexpressed in BL21 (DE3) and BL21 Codon + cells, respectively, lysed using the BugBuster Protein Extraction Reagent (Novagen), and purified by Ni–NTA affinity purification and size exclusion chromatography, as described previously (Siu et al., 2008a; Lee et al., 2001). The following modifications were made to the documented protocols: For the DXMS experiments, 10 mM sodium-HEPES, pH 7.2, 50 mM sodium chloride was used as the final protein elution buffer. For the kinetics, ITC and crystallization experiments, 50 mM sodium-HEPES, pH 7.5 was used as the final protein elution buffer.

2.2. Deuterium–hydrogen exchange coupled mass spectrometry

Prior to conducting the deuterium–hydrogen exchange experiments, the conditions for protein fragmentation under quench conditions were optimized for *Ec*MTAN and *At*MTAN1 as follows: 50 µg of enzyme was diluted into 20 µL of 10 mM sodium-HEPES, pH 7.2, 50 mM sodium chloride. Next, 30 µL of quench buffer consisting of 0.8% (v/v) formic acid, pH 2.3, 16.7% (v/v) glycerol and varying concentrations of guanidine hydrochloride (GuHCl) from 0 to 6.4 M was added. The sample was then digested over a pepsin-conjugated column and peptic fragments were separated by hydrophobicity over a C18 column (C18 300A; Grace Vydac, Hesperia, CA) with a linear acetonitrile gradient from 6.4–38.4%. Eluate was electrosprayed directly into a Thermo Finnigan LCQ Classic ion-trap mass spectrometer (San Jose, CA) for data acquisition. Sequest (Thermo Finnigan Inc.) was used to analyze the MS/MS data. For both *Ec*MTAN and *At*MTAN1, the quench condition that produced the most complete fragment map was 3.2 M GuHCl, 0.8% (v/v) formic acid, pH 2.3, 16.7% (v/v) glycerol.

Deuteration was initiated by diluting 0.7 mg of enzyme into 280 µL of H/D exchange buffer, 10 mM sodium-HEPES, pH_{read} 7.2, 50 mM sodium chloride, final D₂O 75% (v/v) at 4 °C. At 10, 30, 100, 300, 1000 or 3000 s, 20 µL of the reaction cocktail was pipetted into 30 µL of quench buffer (3.2 M GuHCl, 0.8% (v/v) formic acid, pH 2.3, 16.7% (v/v) glycerol). The final protein concentration of the quenched sample was 1 mg/mL. Negative controls were prepared the same way, but with non-deuterated buffers. Equilibrium-exchange samples

were prepared by diluting 50 μg of enzyme into 20 μL of 0.5% (v/v) formic acid, 10 mM sodium-HEPES, 50 mM sodium chloride, 75% (v/v) D_2O , and incubating for 16 h at 22 $^\circ\text{C}$. The hydrogen exchange reaction was stopped by adding 30 μL of quench buffer at 0 $^\circ\text{C}$. All quenched reactions were rapidly frozen on dry ice and stored at -80 $^\circ\text{C}$ until analyzed.

Deuteration levels were analyzed by electrospray ionization mass spectrometry. All steps were performed at 0 $^\circ\text{C}$. Samples were fragmented, separated and analyzed by ion trap MS/MS as described above. The DXMS software from Sierra Analytics was used to calculate the deuterium levels of peptide fragments from the time-course deuteration experiments, as described previously (Burns-Hamuro et al., 2005; Englander et al., 2003; Hamuro et al., 2002a,b, 2003; Zawadzki et al., 2003). In brief, the number of deuterons incorporated was calculated by $(m_p - m_n)/(m_f - m_n) \times \text{MaxD}$, where m_p , m_n and m_f refer to the mass centroid values for partially deuterated, non-deuterated and equilibrium deuterated samples, respectively. MaxD refers to the maximum number of deuterons that can be incorporated and is equal to the number of residues in the fragment subtracted by the number of prolines in the fragment and the first two residues. The first two amino acids of each fragment were omitted from analysis because these amino acids undergo relatively fast H/D exchange and any deuterons incorporated may therefore be lost in the fragmentation and separation steps. The percent deuteration was calculated by $(\text{number of deuterons incorporated})/\text{MaxD} \times 100\%$.

2.3. Generation and kinetic characterization of the *A* Δ MTAN1-Glu202Gln mutant

The *A* Δ MTAN1-Glu202Gln mutant was generated using the Quikchange site-directed mutagenesis kit (Stratagene) and the following forward and reverse primers: 5'GATGCGATTTCCTGTACG TCCCACGACGGCACCGC3' and 5'GCGGTGCCGTCGTGGGACGTACAG GAAATCGCATC3'. The mutant was expressed and purified as described for the wild-type enzyme (Siu et al., 2008a). The integrity and melting temperature of the mutant were determined by circular dichroism. The activity of *A* Δ MTAN1-Glu202Gln was tested using a xanthine oxidase-coupled spectrophotometric assay (Dunn and Bryant, 1994), which measures the amount of the adenine product produced during the reaction. For each molecule of adenine oxidized, two molecules of 2-(4-iodophenyl)-3-(4-nitrophenyl)-5-phenyltetrazolium chloride (INT) are reduced to formazan, a coloured product that absorbs at 470 nm (de Groot et al., 1985). The reactions were performed in 50 mM sodium-HEPES, pH 7.5, using 0.50 μg of *A* Δ MTAN1-Glu202Gln, 0.28 units of xanthine oxidase (Sigma–Aldrich Chemicals) and 0.94 mM of INT (Sigma–Aldrich Chemicals) in a final volume of 800 μL . The concentration of MTA (Sigma–Aldrich Chemicals) or SAH (Sigma–Aldrich Chemicals) was varied from 12.5 μM to 2 mM. As a positive control, wild-type *A* Δ MTAN1 was tested. The reactions were monitored on a Biochrome Ultraspec 2100 UV/Vis spectrophotometer outfitted with the SWIFT II enzyme kinetics software (Amersham Pharmacia Biotech). Changes in absorption at 470 nm were converted to the amount of formazan released using the molar absorption coefficient of 15,400 $\text{M}^{-1} \text{cm}^{-1}$.

2.4. Isothermal titration calorimetry

For the ITC studies, SAH and MTA were dissolved in the HEPES buffer used in the final elution step of protein purification. The protein, substrates and buffers were degassed by gentle stirring under a thermo-vacuum chamber for ten minutes at 24 °C. All experiments were performed in 50 mM sodium-HEPES, pH 7.5, at 25 °C using a VP-ITC microcalorimeter (MicroCal Inc., Northhampton, MA). To determine the thermodynamics of substrate binding, the following concentrations were used: 3 mM SAH was titrated against 0.1 mM (monomer) *A*MTAN1; 3.5 mM ADE was titrated against 0.1 mM (monomer) *A*MTAN1; 4 mM MTA was titrated against 0.1 mM (monomer) *A*MTAN1-Glu202Gln; 5 mM SAH was titrated against 0.6 mM (monomer) *A*MTAN1-Glu202Gln; 4 mM MTA was titrated against 0.09 mM (monomer) *E*cMTAN-Glu174Gln; and 3 mM SAH was titrated against 0.13 mM (monomer) *E*cMTAN-Glu174Gln. The titration experiment of SAH against *A*MTAN1-Glu202Gln consisted of one 2 μ L injection, followed by twelve 20 μ L injections, with a 240 s interval between injections. All other titration experiments consisted of one 2 μ L injection, followed by twenty-eight 10 μ L injections, with a 240 s interval between injections. The injection speed was 0.5 μ L s⁻¹ and the stirring speed was 310 rpm. To account for the heat of dilution, reference data where the ligand was titrated into buffer alone were subtracted from the sample data prior to curve fitting. The negative control of buffer titrated into protein solution was also completed to validate the absence of interaction between the enzymes and the buffer, but this was not subtracted from the test data. The ITC data were analyzed using the Origin v7.0 software (MicroCal Inc., Northhampton, MA) and the single-binding site model was used for fitting.

2.5. Crystallization of *A*MTAN1 in complex with SAH

Prior to crystallization, *A*MTAN1 was concentrated to 10 mg/mL using a Millipore BioMax 10 K Ultrafree-0.5 mL centrifugal concentrator. Crystals of *A*MTAN1 were grown at 25 °C using the hanging drop vapour diffusion technique by mixing 4 μ L of *A*M-TAN1 with 2 μ L of 0.2 M NH₄Cl, 18% (w/v) PEG3350, 15% (v/v) ethylene glycol. Crystals of approximately 0.2 \times 0.3 \times 0.05 mm appeared after nine days. For data collection at -180 °C, the crystals were first soaked in 0.3 mM SAH, 0.2 M NH₄Cl, 18% (w/v) PEG3350, 15% (v/v) ethylene glycol for ten minutes and vitrified in a stream of liquid nitrogen gas. Diffraction data were collected on our in-house X-ray equipment (Rigaku RUH3R rotating anode generator with Osmic optics and a Rigaku R-AXIS IV⁺⁺ image plate) at The Hospital for Sick Children.

2.6. Structural determination and analysis

The diffraction data were reduced using d*TREK (Pflugrath, 1999) and the DREAR program package (Blessing, 1987) was used to apply Bayesian statistics to the data and eliminate negative intensities (Table 2). The structure was solved by molecular replacement using PHASER (McCoy et al., 2007). *A*MTAN1 complexed with the substrate-analogue, 5'-methylthiotubercidin (MTT) (PDB code: 2QTG), was used as a search model after deleting all ligand and water molecules. Non-crystallographic symmetry (NCS) restraints were used throughout refinement on the central α helices and β -sheet of each of the four monomers. The structure of *A*MTAN1-SAH was initially refined by rigid body refinement and restrained refinement in REFMAC (Murshudov et al., 1997), followed by iterative

rounds of manual rebuilding in COOT (Guranowski et al., 1981) alternated with restrained refinement using REFMAC (Murshudov et al., 1997). Once R and R_{free} decreased to below 0.3, water molecules were added to peaks greater than 2σ in the $F_o - F_c$ map using REFMAC (Murshudov et al., 1997) and by manual inspection. The coordinates of SAH were obtained from the RCSB Ligand Expo (Feng et al., 2004). SAH was fitted into electron density using ARP/wARP (Zwart et al., 2004), and the coordinates were refined in subsequent rounds of restrained refinement. The refinement statistics are reported in Table 2. Structural alignments were performed using the PROFIT program written by Smith. The secondary structure propensities of the *Ec*MTAN-ADE and *A α* MTAN1 crystal structures were analyzed using values established by Shortle (2002).

3. Results

3.1. Conformational flexibility of *A α* MTAN1 and *Ec*MTAN as probed by deuterium–hydrogen exchange coupled mass spectrometry

To compare the collective motions and solvent accessibility of *Ec*MTAN and *A α* MTAN1, DXMS experiments were conducted. Pepsin digestion conditions were optimized and the overlapping fragments generated cover the entire length of the protein sequence. Only non-overlapping peptides were selected for analysis to prevent ambiguity. The data among peptide fragments of different lengths were normalized by expressing deuteration levels as a percentage of deuteration rather than in absolute values to allow direct comparison of equivalent peptides from *Ec*MTAN and *A α* MTAN1. As shown in Fig. 2, the peptide fragments exhibit a broad range of deuterium exchange rates. When the peptide exchange rates are mapped onto the structures of *Ec*MTAN and *A α* MTAN1, all fragments that exhibit over 50% deuteration after 300 s of exchange are solvent-exposed (data not shown).

Overall, the hydrogen exchange rates are comparable for the bacterial and plant enzymes (Fig. 2), with significant solvent protection in the core β strands (Fig. 3). The N-terminus of *A α* MTAN1 shows significantly higher deuteration levels compared to *Ec*MTAN, with 100% deuterium incorporation after 100 s of exchange (Fig. 2). In *Ec*MTAN, the N-terminus shows less than 30% deuteration after 3000 s of exchange (Fig. 2). The difference in exchange rates is consistent with the structures of the enzymes. In all of the available crystal structures of *A α* MTAN1, no electron density is observed for the first 19–22 residues. This result implies that the N-terminus is highly mobile, a finding that is supported by secondary structure prediction, which suggests that residues 1–13 and 18–26 likely form random coils (Raghava, 2000). The first 26 residues of *A α* MTAN1 are not present in bacterial MTAN sequences. Instead, the N-terminus of *Ec*MTAN is buried in the central β -sheet, where amide protons are solvent-protected by inter-strand hydrogen bonds.

At the quaternary interface, 10–60% higher deuteration levels are observed in the peptide fragments of *A α* MTAN1 (residues 52–74 and 77–82) compared to *Ec*MTAN (Fig. 2). The increased exchange rates of these fragments in *A α* MTAN1 are not surprising because residues 51–62 and 79–91 form long loops in *A α* MTAN1, but are replaced by much shorter loops comprised of only four and six residues, respectively, in *Ec*MTAN (Fig. 2). Residues 88–97 of *A α* MTAN1 and residues 50–62 of *Ec*MTAN form part of helix α 2 and are deeply

buried at the quaternary interface. Less than 10% deuteration is observed for this region in *EcMTAN* and *A μ MTAN1* after 3000 s of deuterium exchange.

Residues 153–158 of helix α 4 in *EcMTAN* (residues 185–190 in *A μ MTAN1*) are the only part of the quaternary interface that exhibits higher deuteration levels in the bacterial enzyme compared to the plant enzyme (Fig. 2). This region is part of the active site and flanks residues that directly interact with the ligand (e.g. Phe151 in *EcMTAN* and its equivalent residue Leu181 in *A μ MTAN1*). In *EcMTAN*, this region shows >80% deuterium incorporation at all time points (Fig. 2). In *A μ MTAN1*, the corresponding peptide fragment shows >30% deuterium incorporation after 10 s of solvent exchange, with an increase to >80% only after 3000 s (Fig. 2). Like *EcMTAN*, residues 185–190 of helix α 4 in *A μ MTAN1* undergo significant hydrogen–deuterium exchange.

Two additional solvent-exposed regions contribute to the active site. These are the β 10– α 6 and 3_{10} – β 7 loops in *EcMTAN*, which correspond to the β 10– α 6 loop and α 2b helix in *A μ MTAN1*. The peptide fragment that represents the β 10– α 6 region of *EcMTAN* (residues 197–207) exhibits >60% deuteration after 30 s of exchange and becomes fully deuterated after 3000 s of exchange (Fig. 2). The 3_{10} – β 7 region (residues 107–119) exhibits >20% deuteration after 10 s of solvent exchange and >30% after 3000 s of exchange. At all time points, the β 10– α 6 and 3_{10} – β 7 loops of *EcMTAN* show at least 20% higher deuterium incorporation compared to the corresponding regions in *A μ MTAN1* (Fig. 4), indicating higher levels of conformational flexibility in the active site of the bacterial enzyme.

3.2. Crystallographic B factor comparison

One method to cross-validate the results from the mass spectrometry experiments is to compare the rates of deuterium–hydrogen exchange with the B factors from available crystal structures. Crystallographic temperature factors are affected by both crystal packing and conformational disorder, and elevated B factors in certain regions of the molecule suggest increased conformational dynamics (Ringe and Petsko, 1985, 1986). The temperature factors of the crystal structures that represent the open and closed states of each enzyme were scaled such that the average B factors of all protein atoms in all structures are equal to that of the closed state of *A μ MTAN1*. The scaled B factors were then plotted as a function of residue number (Fig. 5). Because an apo structure of *EcMTAN* is not available, the adenine-bound structure (PDB: 1JYS), which is thought to be equivalent to the unbound state, was used to represent the open conformation of *EcMTAN*. The apo structure of *A μ MTAN1* (PDB: 2QSU) was chosen to represent the open conformation of the plant enzyme. Substrate-analogue bound structures of *EcM-TAN* and *A μ MTAN1* are available (PDB: 1NC1 and 2QTG) to represent the closed conformation of the two enzymes.

The B factors of residues in the central β strands (β 4, β 5, β 6, β 8 and β 10) of the open and closed forms of *A μ MTAN1* and *EcMTAN* are on average 17% lower than the rest of the protein. The data correlate well with the DXMS results presented, which demonstrate solvent protection in the core β strands. More importantly, the scaled average B factors of the core β strands in the four crystal structures are within 6% of each other. This gives confidence that the B factors were scaled properly to account for the differences in lattice disorder, because two crystal structures that have comparable lattice disorder are expected to

have roughly equal values for the smallest coordinate displacements, which are represented by the lowest B factors (Ringe and Petsko, 1985). In *A Δ MTAN1*, the greatest change in B factor is observed in the β 10– α 6 region (residues 220–237). It should be noted that B factors for part of the β 10– α 6 region (residues 202–205) in the open state of *EcMTAN* are not available, as the quality of the electron density in this region prevents these residues from being modeled (Lee et al., 2001). It is therefore expected that the change in B factor will be greater in the equivalent residues in *EcMTAN* (residues 193–210). Previous crystallographic studies have suggested that the β 10– α 6 loop of *EcMTAN* undergoes a loop-to-helix transition to form a cap over the active site when a ligand binds (Lee et al., 2003). This change in secondary structure has not been observed in *A Δ MTAN1*. For all other active site residues that directly interact with the ligand, the binding of a ligand results in an average decrease in B factor by 26% in *EcMTAN* (Fig. 5a). In *A Δ MTAN1*, the B factors of the equivalent residues in the closed state are only on average 3% lower than those of the open state (Fig. 5b). The greater difference in B factors between the open and closed conformations of the *EcMTAN* active site compared to *A Δ MTAN1* correlates well with the observation of higher deuteration levels in the *EcMTAN* active site in the DXMS experiments.

3.3. Substrate binding induces a favourable entropic change in *A Δ MTAN1* but unfavourable entropic change in *EcMTAN*

To gain further understanding into the thermodynamics of substrate binding in *EcMTAN* and *A Δ MTAN1*, ITC experiments were conducted (Fig. 6 and Table 1). First, SAH was titrated against *A Δ M-TAN1* to determine if this substrate could bind to the enzyme. When SAH was titrated against *A Δ MTAN1*, the binding isotherms (Fig. 6a) clearly revealed that *A Δ MTAN1* binds but does not hydrolyze SAH. The binding of SAH to *A Δ MTAN1* results in favourable changes in entropy and enthalpy. The dissociation constant was calculated to be in the micromolar range (Table 1, Fig. 6a), approximately 20-fold higher than the K_m of *EcMTAN* for SAH ($1.3 \pm 0.2 \mu\text{M}$). To explore the enthalpic and entropic energy changes associated with MTA binding to *A Δ MTAN1*, an enzymatically inactive *A Δ MTAN1*-Glu202Gln mutant was generated. Characterization of this mutant by circular dichroism showed that the mutant is properly folded with a melting temperature of 68 °C, which is comparable to the melting temperature observed for wild-type *A Δ MTAN1* (74 °C). The binding of MTA to *A Δ MTAN1*-Glu202Gln leads to a favourable change in entropy and unfavourable change in enthalpy (Table 1, Fig. 6d). Titration of SAH into *A Δ MTAN1*-Glu202Gln results in insignificant changes in heat that are less than 0.3 $\mu\text{cal/s}$ (Table 1, Fig. 6c). This indicates that the K_d of SAH for the mutant enzyme is greater than 0.6 mM, the detection limit of the experiment. The catalytic reaction product, adenine, is found to bind *A Δ MTAN1* with comparable affinity as MTA (K_m of $1.5 \pm 0.2 \mu\text{M}$) and approximately 15-fold more tightly than SAH (Table 1, Fig. 6b).

To characterize the binding of substrates to *EcMTAN*, the mutant equivalent to *A Δ MTAN1*-Glu202Gln in *EcMTAN*, *EcMTAN*-Glu174Gln, was overexpressed and purified as previously described (Lee et al., 2005). Titration of SAH or MTA into *EcM-TAN*-Glu174Gln leads to favourable enthalpic and unfavourable entropic changes (Table 1, Fig. 6e and f).

3.4. Crystal structure of *A*MTAN1 in complex with SAH

As previous modeling had suggested that SAH could not be accommodated in the confined active site of the plant enzyme (Siu et al., 2008a) but our ITC results demonstrate unequivocally that *A*MTAN1 can bind SAH, the crystal structure of *A*MTAN1 in complex with SAH was determined (Table 2). Analysis by Molprobity shows that 98% of residues are in the favored regions and no residues fall in the disallowed regions (Lovell et al., 2003). The coordinates and structure factors for *A*MTAN1-SAH have been deposited in the PDB, accession code 3LGS and RCSB057259, respectively. The asymmetric unit contains two *A*MTAN1 dimers. The overall structures of all four monomers are nearly identical, with an average root mean squared (rms) deviation of 0.27 ± 0.09 Å between all main chain atoms. The tertiary structure compares well to previously solved *A*MTAN1 structures (PDB: 2QTG, 2QSU, 2QTT), with rms deviations of less than 0.6 Å between all C α atoms.

With the exception of Glu202, the active site residues are highly superimposable in all four monomers. In monomers B and D, Glu202 assumes a single conformation not previously observed in any of the available MTAN structures (Singh et al., 2006; Siu et al., 2008a,b; Park et al., 2009, 2006; Lee et al., 2001, 2003, 2005). In monomers A and C, an additional conformation is observed at 40% occupancy (Fig. 7a). In these active sites, this second conformation of Glu202 is similar to the orientation of Glu202 observed in all previously determined MTAN structures. In all four monomers, the $3F_o - 2F_c$ map shows strong electron density for the adenine base of SAH (Fig. 7b). At 0.8 sigma, electron density is observed for the glycosidic bond and ribose moiety, but not the 5'-homocysteinyl tail (Fig. 7b). Given the density, we modeled both adenine and SAH in the active site at 50% occupancy. As no electron density was observed for the 5'-substituent of SAH, it was not modeled into the structure. In all four monomers, two water molecules located near the O2' and O3' atoms of SAH are present at 50% occupancy (Fig. 7). In monomers A, B and D, an additional water molecule is present near the S5' atom of SAH at 50% occupancy. The catalytic water molecule, which is present at full occupancy (WAT451, 295, 430 and 227 in monomers A, B, C and D, respectively), is located 4.3 Å from the anomeric carbon and 3.5 Å from O3'.

4. Discussion

Peptide amide deuterium-hydrogen exchange mass spectrometry (DXMS) is based on the principle that labile hydrogens in proteins are in continuous flux with hydrogens in the solvent. The rate of exchange is affected by both protein dynamics and structure, as stable intra- or intermolecular hydrogen-bond interactions protect amide protons from solvent exchange. Increased levels of protein dynamics and conformational flexibility are correlated with higher hydrogen-deuteron exchange rates because transient breakage of hydrogen bonds between residues exposes amide protons to the bulk solvent. By monitoring the increase in mass of purified protein incubated in deuterated solvent, the rate and level of exchange can be determined and this serves as an important source of structural and dynamic information (Burke et al., 2008; Joh et al., 2008; Hsu et al., 2008; Li et al., 2008; Black et al., 2004, 2007; Brock et al., 2007; Yan et al., 2004; Brudler et al., 2006; Golynskiy et al., 2007; Englander, 2006; Carter et al., 2005).

Previous studies have shown that both *Ec*MTAN and *A*MTAN1 exist as stable homodimers in solution. This is reflected in the solvent protection observed for residues 88–97 of *A*MTAN1 and residues 50–62 of *Ec*MTAN, which are buried at the quaternary interface. Less than 10% deuteration is observed for this region in *Ec*MTAN and *A*MTAN1 after 3000 s of deuterium exchange. In general, higher solvent accessibility was expected at the quaternary interface of *A*MTAN1 because this interface contains more polar residues and a greater percentage of the residues are in loop structures. Based on the crystal structure of *A*MTAN1 (PDB code: 2QSU), the Swiss PDB viewer program calculates 44% solvent accessibility to this enzyme's quaternary interface (Guex and Peitsch, 1997). The two monomers of *A*MTAN1 associate *via* a hydrogen bond network involving twelve residues, as well as hydrophobic interactions contributed by eight non-polar residues and π - π stacking interactions between Trp62 and Phe100. In contrast, the Swiss PDB view program estimates that only 39% of the *Ec*MTAN quaternary interface (PDB: 1JYS) is solvent-accessible. In *Ec*MTAN, the residues involved in quaternary interactions are predominantly hydrophobic; sixteen non-polar residues interact *via* hydrophobic interactions and only four polar residues contribute to hydrogen-bond interactions. The current DXMS results are consistent with the structural findings. Helix α 4 is located near the intersubunit interface and is part of the active site. Given that helix α 4 of *Ec*MTAN contains only one residue with amide protons in the side chain (Asn153), the observed 80% deuterium incorporation in the corresponding peptide suggests that this helix undergoes partial unfolding to expose backbone amide protons to the solvent. The crystal structures of *Ec*MTAN and *A*MTAN1 show that helix α 4 of the plant enzyme is partially buried at the quaternary interface while that of the bacterial enzyme is completely solvent-exposed. This explains the observed partial protection from solvent in helix α 4 of *A*MTAN1 and near-complete deuteration in *Ec*MTAN.

Previous structural studies suggest that in *Ec*MTAN, the binding of a ligand induces a loop-to-helix transition in the β 10- α 6 loop, which forms a cap over the active site and allows residues in this region to directly interact with the bound ligand (Lee et al., 2003). Also, the 3_{10} - β 7 loop has been proposed to migrate approximately 3 Å towards the neighbouring subunit on ligand binding to form a cap over the substrate (Lee et al., 2003). In *A*MTAN1, the binding of a ligand induces small C α displacements of less than 1.5 Å in the β 10- α 6 loop and α 2 $_b$ helix (Siu et al., 2008a). Our current analysis of the B factors and our DXMS results confirm that these regions are likely more disordered in *Ec*MTAN than in *A*MTAN1. The difference in B factors in the active site residues between the open and closed conformations is significantly greater in *Ec*MTAN than in *A*MTAN1, suggesting a greater change in conformational disorder between the open and closed states of the bacterial enzyme. Comparison of the secondary structure propensities reveals that residues in the α 6 helix of *A*MTAN1 have higher propensity to form α helical structure compared to the corresponding region in *Ec*MTAN (data not shown). The DXMS results clearly demonstrate that a higher relative population of *Ec*MTAN than *A*MTAN1 adopts conformations that allow the active site residues to undergo solvent exchange. At all time points, at least 20% higher deuterium incorporation was observed in the β 10- α 6 and 3_{10} - β 7 regions of *Ec*MTAN compared to *A*MTAN1. While the experiments do not probe dynamics at catalytic

timescales, it is reasonable to postulate that higher collective motions exist in the active site of the bacterial enzyme and this premise is substantiated by our ITC studies.

ITC allows direct measurement of heat evolved or absorbed as a result of an interaction event. If the stoichiometry and initial concentrations of the interacting species are known, the dissociation constant (K_d), in addition to the changes in enthalpy (ΔH) and entropy (ΔS), can be determined. The binding of MTA or SAH to *Ec*MTAN-Glu174Gln leads to favourable changes in enthalpy. Likewise, the binding of SAH or ADE to *A*MTAN1 is enthalpically favourable, but the binding of MTA to *A*MTAN1-Glu202Gln leads to a ΔH of 5.6 ± 0.3 kcal/mol (Table 1, Fig. 6d). An unfavourable binding enthalpy typically indicates that interactions between the enzyme and ligand are not strong enough to compensate for the unfavourable enthalpy associated with desolvation (Freire, 2008). Mutating Glu202 to Gln results in the loss of two favourable hydrogen-bond interactions with the hydroxyl groups of MTA and unfavourable interactions are potentially introduced. These changes in hydrogen-bond interactions are sufficient to account for the observed difference in enthalpy changes associated with the binding of a ligand to wild-type versus mutant *A*MTAN1. Binding of SAH to the *A*MTAN1-Glu202Gln mutant was not detected. As depicted in our current crystal structure of *A*MTAN1 in complex with SAH, interactions between the wild-type enzyme and SAH are made *via* the adenine- and ribose-groups, and no stable interactions with the 5'-homocysteiny tail are observed (Fig. 8a and b). Mutating Glu202 to Gln perturbs the hydrogen-bond interactions with the ribose moiety, and thereby diminishes the mutant's ability to bind SAH. Mutating the equivalent residue in *Ec*MTAN, Glu174, to Gln likely also negatively impacts ligand interactions. However, compared to *A*MTAN1, *Ec*MTAN makes more and stronger direct hydrogen-bond interactions to the adenine- and ribose-groups of the bound ligand (Siu et al., 2008a), so despite the Glu-to-Gln mutation, favourable enzyme-ligand interactions outweigh the enthalpic penalty of desolvation.

The interaction of both MTA and SAH with *Ec*MTAN is entropically unfavourable. Entropic penalties account for changes in solvent order, hydrophobic interactions and dynamics of both the bound ligand and protein, with the predominant contribution coming from changes in protein dynamics. Previous crystallographic studies have shown that the binding of a ligand displaces all except for the catalytic water molecule from the active site of *Ec*MTAN (Lee et al., 2003). As water molecules are released into the bulk solvent, they gain freedom of movement and this causes a favourable change in entropy. The observed entropic penalty upon ligand binding in *Ec*MTAN indicates that the burial of fluidic surface residues at the ligand-enzyme interface results in a decrease in conformational disorder that exceeds the favourable entropic change from solvent release. Unlike *Ec*MTAN, the binding of a substrate to *A*MTAN1 is an entropically favourable event. Available crystal structures show that the active site of *A*MTAN1 remains partially hydrated in ligand-bound state. This means the binding of a substrate to *A*MTAN1 leads to only small changes in conformational disorder that do not exceed the gain in entropy from solvent release. The binding of the catalytic reaction product, adenine, to *A*MTAN1 is entropically unfavourable. This is reasonable because crystal structures (PDB: 2H8G, 2QSU) have shown that the binding of a substrate-analogue to *A*MTAN1 displaces five water molecules from the active site while adenine displaces only two. The binding of adenine rigidifies the active site and causes a loss of entropy that is not sufficiently compensated by solvent release.

Our ITC experiments clearly show that SAH is able to bind *A*MTAN1 with a dissociation constant of $24.8 \pm 2.6 \mu\text{M}$. This result was unexpected because when SAH was modeled into the crystal structures of *A*MTAN1, it appeared that residues in the 5'-alkylthio binding site would sterically clash with the homocysteiny tail of SAH and no favourable electrostatic interactions could be established (Siu et al., 2008a; Park et al., 2006). To understand how SAH binds and why *A*MTAN1 cannot hydrolyze the substrate, the crystal structure of *A*MTAN1 in complex with SAH was determined. The 2.2-Å crystal structure of *A*MTAN1-SAH shows that adenine and SAH are both present in the active site at 50% occupancy. Since adenine is ubiquitous in the cytoplasm of *E. coli* and *A*MTAN1 binds adenine with a dissociation constant of $1.7 \mu\text{M}$ (Table 1, Fig. 6d), the nucleobase may have been salvaged from the cytosol during purification and co-crystallized with the enzyme. Previous crystallographic studies of MTANs have found adenine bound in the active site even though the nucleobase was not added to the crystallization condition (Park et al., 2009, 2006; Lee et al., 2001). Although the *A*MTAN1 crystals were soaked in high concentrations of SAH, adenine has a 15-fold higher affinity for *A*MTAN1 than SAH, so it is possible that SAH molecules displaced adenine from only approximately half of the protein molecules and the rest remained bound by adenine. Another possibility is that some SAH molecules were hydrolyzed during the short soak of 10 min prior to crystal vitrification and data collection. This second scenario is less likely given that both our kinetics and ITC studies, which were conducted over 10- and 30-min durations, respectively, did not detect catalytic activity in *A*MTAN1 towards SAH. None of the active site residues are involved in crystallographic contacts, so it is unlikely that the enzyme is forced into a conformation that allows hydrolysis or affects binding of SAH.

Catalysis by MTAN involves three key residues. In *A*MTAN1, Asp225 is the proposed catalytic acid and donates a proton to the N7 atom of the substrate. The adenine ring draws electrons from the ribosyl group, which causes the glycosidic bond to elongate and substantial positive charge to build up on the ribosyl group. This partial positive charge is stabilized by the catalytic water molecule (WAT3) and Glu202, which polarizes the O3' to create a partial negative charge. The catalytic water molecule then becomes activated by Glu38 and attacks the anomeric carbon of the oxacarbenium-like intermediate to form the catalytic products (Lee et al., 2005). The importance of these residues to catalysis has been demonstrated in mutagenesis studies, which show that mutating Asp225, Glu38 or Glu202 in *A*MTAN1 to alanine completely abolishes catalytic activity in *A*MTAN1 (data not shown). Similarly, mutating the equivalent residues in *Ec*MTAN renders the enzyme inactive (Lee et al., 2005). In the structure of *A*MTAN1-SAH, Glu202 assumes a single conformation in monomers B and D (Fig. 7a). This will be referred to as the dominant orientation of Glu202 and is different from that observed in all previously determined MTAN structures. While two conformations are observed in subunits A and C, the second alternate conformation is only present at 40% occupancy. This second alternate conformation is similar to that observed previously, and may reflect the presence of adenine rather than SAH in some active sites. In the dominant conformation, Glu202 does not interact with the bound ligand directly (Fig. 7). Instead, it only makes a water-mediated hydrogen bond with the 3'-hydroxyl group (Fig. 8a). In previously determined crystal structures of *A*MTAN1 in complex with substrate and transition-state-analogues (PDB codes: 2QTG and 2QTT), WAT3 makes a 2.8

Å (2.4–2.9 Å in *Ec*MTAN structures) hydrogen bond with the 3'-OH of the ligand and has been suggested to play a role in stabilizing the oxacarbenium intermediate (Fig. 8c) (Siu et al., 2008a). In the current SAH-complexed structure, at 3.5 Å away, WAT3 is located beyond hydrogen bonding distance from the 3'-OH of SAH. Since withdrawal of electrons from the adenine group and optimal stabilization of the oxacarbenium anion intermediate cannot be achieved, it is unlikely that catalysis can take place. The lack of electron density for the 5'-substituent of SAH indicates that this region is completely disordered. The residues in the 5'-binding pocket of *A*MTAN1 are hydrophobic so favourable electrostatic interactions with the carboxyl group of the 5'-homocysteiny tail cannot be established. Despite suboptimal binding in the 5'-alkylthio region and the loss of one hydrogen bond to Glu202, SAH shows significant affinity for *A*MTAN1 because all other interactions in the adenine- and ribose-binding subsites are maintained (Fig. 8). The loss of hydrogen bond interaction with Glu202 may be compensated by a new hydrogen bond interaction that is formed between Thr116 and the ribosyl O4' (Fig. 7).

The importance of subtle residue motion to catalytic activity has been demonstrated in other systems such as DNA polymerases. Experimental and theoretical studies on DNA polymerase β have shown that the binding of a substrate-analogue with a mismatched base hinders the changes in protein conformation that are necessary for the subsequent chemical step, and that subtle conformational changes in individual residues are critical to substrate discrimination and polymerase fidelity (Radhakrishnan et al., 2006). Our current results offer an alternative to the previous hypothesis that *A*MTAN1 selects against SAH primarily based on the size of the 5'-substituent (Siu et al., 2008a; Park et al., 2009). We have shown *via* DXMS and ITC studies that the active site of *A*MTAN1 is less accessible to solvent than that of *Ec*MTAN, but this does not hamper the binding of SAH to the plant enzyme. Also, previous kinetics studies have shown that *A*MTAN1 can hydrolyze substrates with extended 5'-substituents, such as 5'-isobutylthioadenosine, 5'-butylthioadenosine and 5'-iodoadenosine (Siu et al., 2008a). This lends support to our argument that the enlarged 5'-alkylthio binding cavity of *A*MTAN2 may not be the main discriminating factor for activity towards SAH. Instead, subtle differences in the way the enzyme binds SAH may be responsible for substrate specificity. The structure of *A*MTAN1 in complex with SAH suggests that binding of SAH changes the positions of the catalytic water molecule, WAT3, and Glu202. If so, Glu202 and the catalytic water molecule cannot perform their catalytic functions of polarizing and stabilizing the transition state intermediate, thus rendering hydrolysis impossible. Dynamics may play a role in substrate specificity because higher conformational flexibility in the active site of *Ec*MTAN may allow displacement of unfavourable interactions and binding of SAH in the active conformation. Bacterial MTANs likely have relatively high levels of conformational flexibility in the active site, while the plant enzymes may have intermediate to low levels of conformational flexibility corresponding to the level of catalytic activity towards SAH.

Acknowledgments

The authors would like to thank G. David Smith, Yura Lobsanov and Dante Neculai for helpful discussions on the structure determination, and Frank Sicheri for access to the isothermal titration calorimeter and software for data analysis. This work is supported by research grants from the Canadian Institutes of Health Research (CIHR) to P.L.H. (#43998), and by grants from the Innovative Technologies for the Molecular Analysis of Cancer (IMAT)

program (CA099835, and CA118595) and NIH Grant (AI076961, AI081982, AI2008031, GM020501, GM066170, and RR029388) to V.L.W. P.L.H. is the recipient of a Canada Research Chair; K.K.W.S. has been supported, fully or in part, by a Master's research award from the Natural Sciences and Engineering Research Council of Canada (NSERC), a studentship from the Ontario Student Opportunities Trust Fund and The Hospital for Sick Children Foundation Student Scholarship Program, and a Canada Graduate scholarship from CIHR.

Abbreviations

MTA	5'-methylthioadenosine
SAH	S-adenosylhomocysteine
AtMTAN1	<i>Arabidopsis thaliana</i> 5'-methylthioadenosine/S-adenosylhomocysteine nucleosidase 1
AtMTAN2	<i>Arabidopsis thaliana</i> 5'-methylthioadenosine/S-adenosylhomocysteine nucleosidase 2
EcMTAN	<i>Escherichia coli</i> 5'-methylthioadenosine/S-adenosylhomocysteine nucleosidase
DXMS	deuterium–hydrogen exchange coupled mass spectrometry
ITC	isothermal titration calorimetry
PDB	Protein Data Bank
RCSB	Research Collaboratory for Structural Bioinformatics
LB	Luria–Bertani broth
IPTG	isopropyl thiogalactoside
PMSF	phenylmethylsulfonyl fluoride
HEPES	4-(2-hydroxyethyl)-1-piperazineethanesulfonic acid
INT	2-(4-iodophenyl)-3-(4-nitrophenyl)-5-phenyltetrazolium chloride
GuHCl	guanidine hydrochloride
MTT	5'-methylthiotubercidin
NCS	non-crystallographic symmetry

References

- Baur AH, Yang SF. Methionine metabolism in apple tissue in relation to ethylene biosynthesis. *Phytochemistry*. 1972; 11:3207–3214.
- Baxter C, Coscia CJ. In vitro synthesis of spermidine in the higher plant, *Vinca rosea*. *Biochem Biophys Res Commun*. 1973; 54:147–154. [PubMed: 4741562]
- Black BE, Foltz DR, Chakravarthy S, Luger K, Woods VL Jr, Cleveland DW. Structural determinants for generating centromeric chromatin. *Nature*. 2004; 430:578–582. [PubMed: 15282608]
- Black BE, Brock MA, Bedard S, Woods VL Jr, Cleveland DW. An epigenetic mark generated by the incorporation of CENP-A into centromeric nucleosomes. *Proc Natl Acad Sci USA*. 2007; 104:5008–5013. [PubMed: 17360341]

- Blessing R. Data reduction and error analysis for accurate single crystal diffraction intensities. *Crystallog Rev.* 1987;3–58.
- Borchardt, R., Creveling, C., Ueland, P. *Biological Methylation and Drugdesign Experimental and Clinical Roles of S-adenosylmethionine.* Humana Press; Clifton, NJ: 1986.
- Brock M, Fan F, Mei FC, Li S, Gessner C, Woods VL Jr, Cheng X. Conformational analysis of Epac activation using amide hydrogen/deuterium exchange mass spectrometry. *J Biol Chem.* 2007; 282:32256–32263. [PubMed: 17785454]
- Brudler R, Gessner CR, Li S, Tyndall S, Getzoff ED, Woods VL Jr. PAS domain allostery and light-induced conformational changes in photoactive yellow protein upon I2 intermediate formation. Probed with enhanced hydrogen/deuterium exchange mass spectrometry. *J Mol Biol.* 2006; 363:148–160. [PubMed: 16952373]
- Burke JE, Karbarz MJ, Deems RA, Li S, Woods VL Jr, Dennis EA. Interaction of group IA phospholipase A2 with metal ions and phospholipid vesicles probed with deuterium exchange mass spectrometry. *Biochemistry.* 2008; 47:6451–6459. [PubMed: 18500818]
- Burns-Hamuro LL, Hamuro Y, Kim JS, Sigala P, Fayos R, Stranz DD, Jennings PA, Taylor SS, Woods VL Jr. Distinct interaction modes of an AKAP bound to two regulatory subunit isoforms of protein kinase A revealed by amide hydrogen/deuterium exchange. *Protein Sci.* 2005; 14:2982–2992. [PubMed: 16260760]
- Burstenbinder K, Rzewuski G, Wirtz M, Hell R, Sauter M. The role of methionine recycling for ethylene synthesis in Arabidopsis. *Plant J.* 2007; 49:238–249. [PubMed: 17144895]
- Carter JM, Gurevich VV, Prossnitz ER, Engen JR. Conformational differences between arrestin2 and pre-activated mutants as revealed by hydrogen exchange mass spectrometry. *J Mol Biol.* 2005; 351:865–878. [PubMed: 16045931]
- Chen X, Schauder S, Potier N, Van Dorsselaer A, Pelczer I, Bassler BL, Hughson FM. Structural identification of a bacterial quorum-sensing signal containing boron. *Nature.* 2002; 415:545–549. [PubMed: 11823863]
- Cornell KA, Swarts WE, Barry RD, Riscoe MK. Characterization of recombinant Escherichia coli 5'-methylthioadenosine/S-adenosylhomocysteine nucleosidase: analysis of enzymatic activity and substrate specificity. *Biochem Biophys Res Commun.* 1996; 228:724–732. [PubMed: 8941345]
- Cruikshank DW. Remarks about protein structure precision. *Acta Crystallogr D Biol Crystallogr.* 1999; 55:583–601. [PubMed: 10089455]
- de Groot H, de Groot H, Noll T. Enzymic determination of inorganic phosphates, organic phosphates and phosphate-liberating enzymes by use of nucleoside phosphorylase-xanthine oxidase (dehydrogenase)-coupled reactions. *Biochem J.* 1985; 230:255–260. [PubMed: 2996493]
- DeLano, WL. *The PyMOL Molecular Graphics System.* v.0.97. DeLano Scientific; San Carlos, CA, USA: 2002.
- Della Ragione F, Porcelli M, Carteni-Farina M, Zappia V, Pegg AE. Escherichia coli S-adenosylhomocysteine/5'-methylthioadenosine nucleosidase. Purification, substrate specificity and mechanism of action. *Biochem J.* 1985; 232:335–341. [PubMed: 3911944]
- Dunn S, Bryant J. A simple spectrophotometric assay for plant 5'-deoxy-5'-methylthioadenosine nucleosidase using xanthine oxidase as a coupling enzyme. *Phytochem Anal.* 1994; 5:286–293.
- Englander SW. Hydrogen exchange and mass spectrometry: a historical perspective. *J Am Soc Mass Spectrom.* 2006; 17:1481–1489.
- Englander JJ, Del Mar C, Li W, Englander SW, Kim JS, Stranz DD, Hamuro Y, Woods VL Jr. Protein structure change studied by hydrogen-deuterium exchange, functional labeling, and mass spectrometry. *Proc Natl Acad Sci USA.* 2003; 100:7057–7062. [PubMed: 12773622]
- Feng Z, Chen L, Maddula H, Akcan O, Oughtred R, Berman HM, Westbrook J. Ligand Depot: a data warehouse for ligands bound to macromolecules. *Bioinformatics.* 2004; 20:2153–2155. [PubMed: 15059838]
- Freire E. Do enthalpy and entropy distinguish first in class from best in class? *Drug Discov Today.* 2008; 13:869–874. [PubMed: 18703160]
- Golynskiy M, Li S, Woods VL Jr, Cohen SM. Conformational studies of the manganese transport regulator (MntR) from Bacillus subtilis using deuterium exchange mass spectrometry. *J Biol Inorg Chem.* 2007; 12:699–709. [PubMed: 17342524]

- Gouet P, Courcelle E, Stuart DI, Metoz F. ESPript: analysis of multiple sequence alignments in PostScript. *Bioinformatics*. 1999; 15:305–308. [PubMed: 10320398]
- Guex N, Peitsch MC. SWISS-MODEL and the Swiss-PdbViewer: an environment for comparative protein modeling. *Electrophoresis*. 1997; 18:2714–2723. [PubMed: 9504803]
- Guranowski AB, Chiang PK, Cantoni GL. 5'-Methylthioadenosine nucleosidase. Purification and characterization of the enzyme from *Lupinus luteus* seeds. *Eur J Biochem*. 1981; 114:293–299. [PubMed: 6783408]
- Hamuro Y, Burns L, Canaves J, Hoffman R, Taylor S, Woods V. Domain organization of D-AKAP2 revealed by enhanced deuterium exchange-mass spectrometry (DXMS). *J Mol Biol*. 2002a; 321:703–714. [PubMed: 12206784]
- Hamuro Y, Wong L, Shaffer J, Kim JS, Stranz DD, Jennings PA, Woods VL Jr, Adams JA. Phosphorylation driven motions in the COOH-terminal Src kinase, CSK, revealed through enhanced hydrogen-deuterium exchange and mass spectrometry (DXMS). *J Mol Biol*. 2002b; 323:871–881. [PubMed: 12417200]
- Hamuro Y, Zawadzki KM, Kim JS, Stranz DD, Taylor SS, Woods VL Jr. Dynamics of cAPK type IIbeta activation revealed by enhanced amide H/2H exchange mass spectrometry (DXMS). *J Mol Biol*. 2003; 327:1065–1076. [PubMed: 12662931]
- Hsu YH, Burke JE, Stephens DL, Deems RA, Li S, Asmus KM, Woods VL Jr, Dennis EA. Calcium binding rigidifies the C2 domain and the intradomain interaction of GIVA phospholipase A2 as revealed by hydrogen/deuterium exchange mass spectrometry. *J Biol Chem*. 2008; 283:9820–9827. [PubMed: 18211893]
- Joh NH, Min A, Faham S, Whitelegge JP, Yang D, Woods VL, Bowie JU. Modest stabilization by most hydrogen-bonded side-chain interactions in membrane proteins. *Nature*. 2008
- Lee JE, Cornell KA, Riscoe MK, Howell PL. Expression, purification, crystallization and preliminary X-ray analysis of *Escherichia coli* 5'-methylthioadenosine/S-adenosylhomocysteine nucleosidase. *Acta Crystallogr D Biol Crystallogr*. 2001; 57:150–152. [PubMed: 11134941]
- Lee JE, Cornell KA, Riscoe MK, Howell PL. Structure of *E. coli* 5'-methylthioadenosine/S-adenosylhomocysteine nucleosidase reveals similarity to the purine nucleoside phosphorylases. *Structure*. 2001; 9:941–953. [PubMed: 11591349]
- Lee JE, Cornell KA, Riscoe MK, Howell PL. Structure of *Escherichia coli* 5'-methylthioadenosine/S-adenosylhomocysteine nucleosidase inhibitor complexes provide insight into the conformational changes required for substrate binding and catalysis. *J Biol Chem*. 2003; 278:8761–8770. [PubMed: 12496243]
- Lee JE, Luong W, Huang DJ, Cornell KA, Riscoe MK, Howell PL. Mutational analysis of a nucleosidase involved in quorum-sensing autoinducer-2 biosynthesis. *Biochemistry*. 2005; 44:11049–11057. [PubMed: 16101288]
- Lee JE, Smith GD, Horvatin C, Huang DJ, Cornell KA, Riscoe MK, Howell PL. Structural snapshots of MTA/AdoHcy nucleosidase along the reaction coordinate provide insights into enzyme and nucleoside flexibility during catalysis. *J Mol Biol*. 2005; 352:559–574. [PubMed: 16109423]
- Li J, Lim MS, Li S, Brock M, Pique ME, Woods VL Jr, Craig L. *Vibrio cholerae* toxin-coregulated pilus structure analyzed by hydrogen/deuterium exchange mass spectrometry. *Structure*. 2008; 16:137–148. [PubMed: 18184591]
- Lovell SC, Davis IW, Arendall WB 3rd, de Bakker PI, Word JM, Prisant MG, Richardson JS, Richardson DC. Structure validation by Calpha geometry: phi, psi and Cbeta deviation. *Proteins*. 2003; 50:437–450. [PubMed: 12557186]
- McCoy AJ, Grosse-Kunstleve RW, Adams PD, Winn MD, Storoni LC, Read RJ. Phaser crystallographic software. *J Appl Crystallogr*. 2007; 40:658–674. [PubMed: 19461840]
- Murshudov GN, Vagin AA, Dodson EJ. Refinement of macromolecular structures by the maximum-likelihood method. *Acta Crystallogr D Biol Crystallogr*. 1997; 53:240–255. [PubMed: 15299926]
- Pajula RL, Raina A. Methylthioadenosine, a potent inhibitor of spermine synthase from bovine brain. *FEBS Lett*. 1979; 99:343–345. [PubMed: 428559]
- Park EY, Oh S, Nam MJ, Shin JS, Kim K, Song HK. Crystal structure of 5'-Methylthioadenosine Nucleosidase from *Arabidopsis thaliana* at 1.5-Å Resolution. *Proteins: Structure, Function and Bioinformatics*. 2006:65.

- Park EY, Choi WS, Oh SI, Kim KN, Shin JS, Song HK. Biochemical and structural characterization of 5'-methylthioadenosine nucleosidases from *Arabidopsis thaliana*. *Biochem Biophys Res Commun*. 2009; 381:619–624. [PubMed: 19249293]
- Pflugrath JW. The finer things in X-ray diffraction data collection. *Acta Crystallogr D Biol Crystallogr*. 1999; 55:1718–1725. [PubMed: 10531521]
- Radhakrishnan R, Arora K, Wang Y, Beard WA, Wilson SH, Schlick T. Regulation of DNA repair fidelity by molecular checkpoints: “gates” in DNA polymerase beta’s substrate selection. *Biochemistry*. 2006; 45:15142–15156. [PubMed: 17176036]
- Raghava GPS. Protein secondary structure prediction using nearest neighbour and neural network approach. *CASP*. 2000; 4:75–76.
- Raina A, Tuomi K, Pajula RL. Inhibition of the synthesis of polyamines and macromolecules by 5'-methylthioadenosine and 5'-alkylthiotubercidins in BHK21 cells. *Biochem J*. 1982; 204:697–703. [PubMed: 6896990]
- Ringe D, Petsko GA. Mapping protein dynamics by X-ray diffraction. *Prog Biophys Mol Biol*. 1985; 45:197–235. [PubMed: 3892584]
- Ringe D, Petsko GA. Study of protein dynamics by X-ray diffraction. *Methods Enzymol*. 1986; 131:389–433. [PubMed: 3773767]
- Riscoe MK, Ferro AJ, Fitchen JH. Methionine recycling as a target for antiprotozoal drug development. *Parasitol Today*. 1989; 5:330–333. [PubMed: 15463143]
- Roje S. S-Adenosyl-L-methionine: beyond the universal methyl group donor. *Phytochemistry*. 2006; 67:1686–1698. [PubMed: 16766004]
- Rzewuski G, Cornell KA, Rooney L, Burstenbinder K, Wirtz M, Hell R, Sauter M. OsMTN encodes a 5'-methylthioadenosine nucleosidase that is upregulated during submergence-induced ethylene synthesis in rice (*Oryza sativa* L.). *J Exp Bot*. 2007; 58:1505–1514. [PubMed: 17339651]
- Schauder S, Shokat K, Surette MG, Bassler BL. The LuxS family of bacterial autoinducers: biosynthesis of a novel quorum-sensing signal molecule. *Mol Microbiol*. 2001; 41:463–476. [PubMed: 11489131]
- Shortle D. Composites of local structure propensities: evidence for local encoding of long-range structure. *Protein Sci*. 2002; 11:18–26. [PubMed: 11742118]
- Singh V, Shi W, Almo SC, Evans GB, Furneaux RH, Tyler PC, Painter GF, Lenz DH, Mee S, Zheng R, Schramm VL. Structure and inhibition of a quorum sensing target from *Streptococcus pneumoniae*. *Biochemistry*. 2006; 45:12929–12941. [PubMed: 17059210]
- Siu KK, Lee JE, Sufrin JR, Moffatt BA, McMillan M, Cornell KA, Isom C, Howell PL. Molecular determinants of substrate specificity in plant 5'-methylthioadenosine nucleosidases. *J Mol Biol*. 2008a; 378:112–128. [PubMed: 18342331]
- Siu KKW, Lee JE, Smith GD, Horvatin-Mrakovic C, Howell PL. Structure of *Staphylococcus aureus* 5'-methylthioadenosine/Sadenosylhomocysteine nucleosidase. *Acta Crystallogr Sec F*. 2008b; 64:343–350.
- Sufrin JR, Meshnick SR, Spiess AJ, Garofalo-Hannan J, Pan XQ, Bacchi CJ. Methionine recycling pathways and antimicrobial drug design. *Antimicrob Agents Chemother*. 1995; 39:2511–2515. [PubMed: 8585735]
- Yan X, Watson J, Ho PS, Deinzer ML. Mass spectrometric approaches using electrospray ionization charge states and hydrogen-deuterium exchange for determining protein structures and their conformational changes. *Mol Cell Proteomics*. 2004; 3:10–23. [PubMed: 14623985]
- Zawadzki KM, Hamuro Y, Kim JS, Garrod S, Stranz DD, Taylor SS, Woods VL Jr. Dissecting interdomain communication within cAPK regulatory subunit type IIbeta using enhanced amide hydrogen/deuterium exchange mass spectrometry (DXMS). *Protein Sci*. 2003; 12:1980–1990. [PubMed: 12930997]
- Zwart PH, Langer GG, Lamzin VS. Modelling bound ligands in protein crystal structures. *Acta Crystallogr D Biol Crystallogr*. 2004; 60:2230–2239. [PubMed: 15572776]

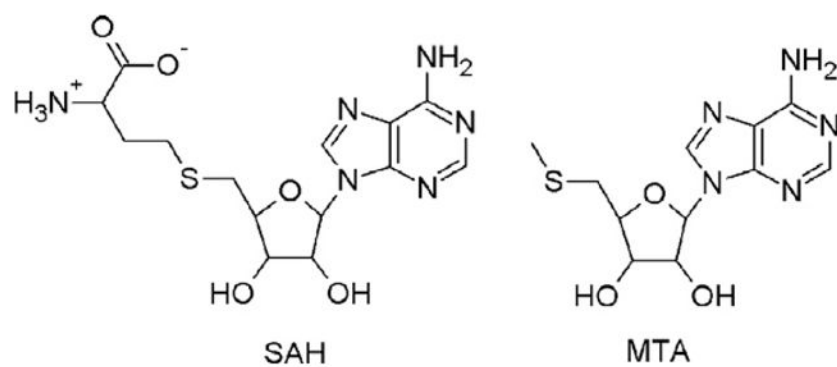


Fig. 1. Structures of S-adenosylhomocysteine (SAH) and 5'-methylthioadenosine (MTA).

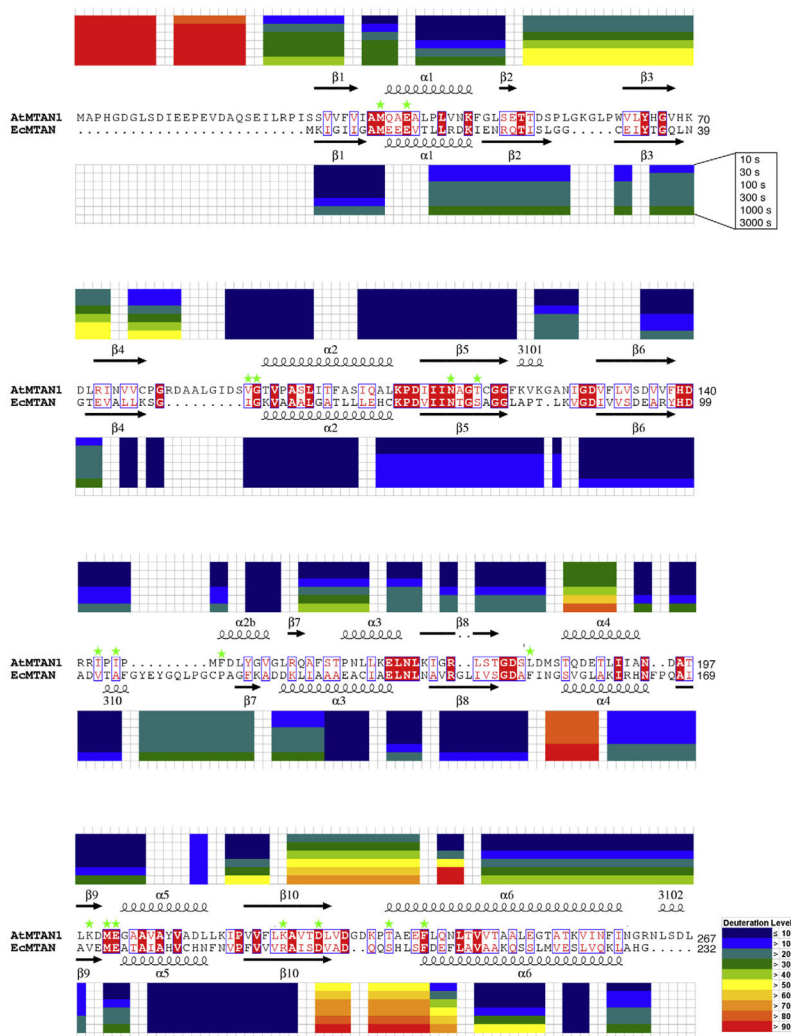


Fig. 2. Time-course percent deuteration of *AaMTAN1* and *EcMTAN1*. Deuteration levels are mapped onto the sequence and structural alignment. The structural topologies at the top and bottom of the alignment correspond to *AaMTAN1* and *EcMTAN1*, respectively. Residues that are strictly conserved are displayed in white in a red box, while residues that are conservatively substituted are displayed in red. Residues that are similar are framed in blue. Residues involved in ligand binding are marked with green asterisks. The alignment was generated using ESPript (Gouet et al., 1999). Time-course experiments of 10, 30, 100, 300, 1000 and 3000 s of deuteron exchange are shown from top to bottom. The residue numbers for each peptide are indicated on top and below the *AaMTAN1* and *EcMTAN1* peptides, respectively.

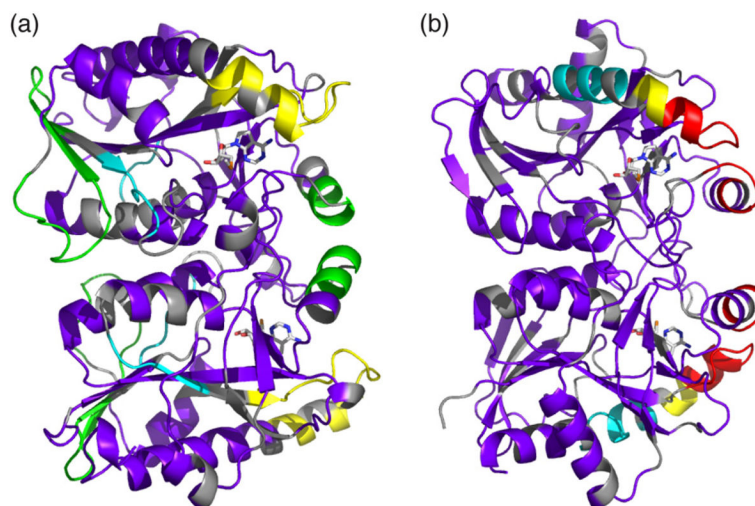


Fig. 3. Hydrogen exchange profiles of *AΔMTAN1* and *EcMTAN*. Hydrogen exchange profiles mapped onto the crystal structures of (a) *AΔMTAN1* and (b) *EcMTAN*. Regions that show 50% deuteration after 10, 300, 1000 and 3000 s of exchange are coloured in red, yellow, green and cyan, respectively. Regions that demonstrate <50% deuteration after 3000 s of exchange are illustrated in purple. Residues shown in gray are not covered in the fragmentation maps. Residues 1–22 and 1–21 are not modeled in the top and bottom subunits, respectively, of the *AΔMTAN1* structure. MTT is modeled in sticks format to depict the active sites. The figure was prepared by PYMOL (DeLano, 2002). (For interpretation of the references to colour in this figure legend, the reader is referred to the web version of this article.)

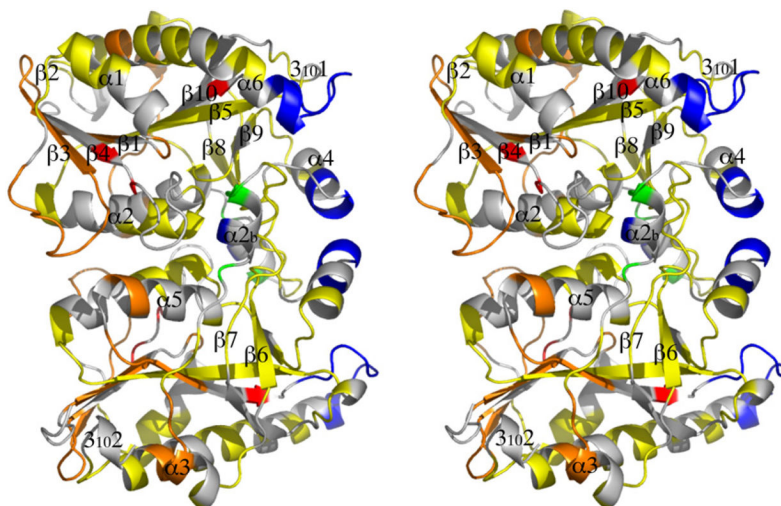


Fig. 4. Stereodiagram of differences in solvent-accessibility between *A*MTAN1 and *Ec*MTAN. At all time points, the deuteration levels of peptides in *A*MTAN1 were subtracted by the deuteration levels found in equivalent peptides in *Ec*MTAN. The average differences are represented as follows: Blue and green indicate a decrease in deuteration of $\sim 20\%$ and $10\text{--}20\%$, respectively; yellow indicates a difference in deuteration of less than 10% ; orange and red indicate an increase in deuteration of $10\text{--}20\%$ and $\sim 20\%$, respectively; gray indicates regions where deuteration data are not available for both enzymes. The stereodiagram was prepared using PYMOL (DeLano, 2002). (For interpretation of the references to colour in this figure legend, the reader is referred to the web version of this article.)

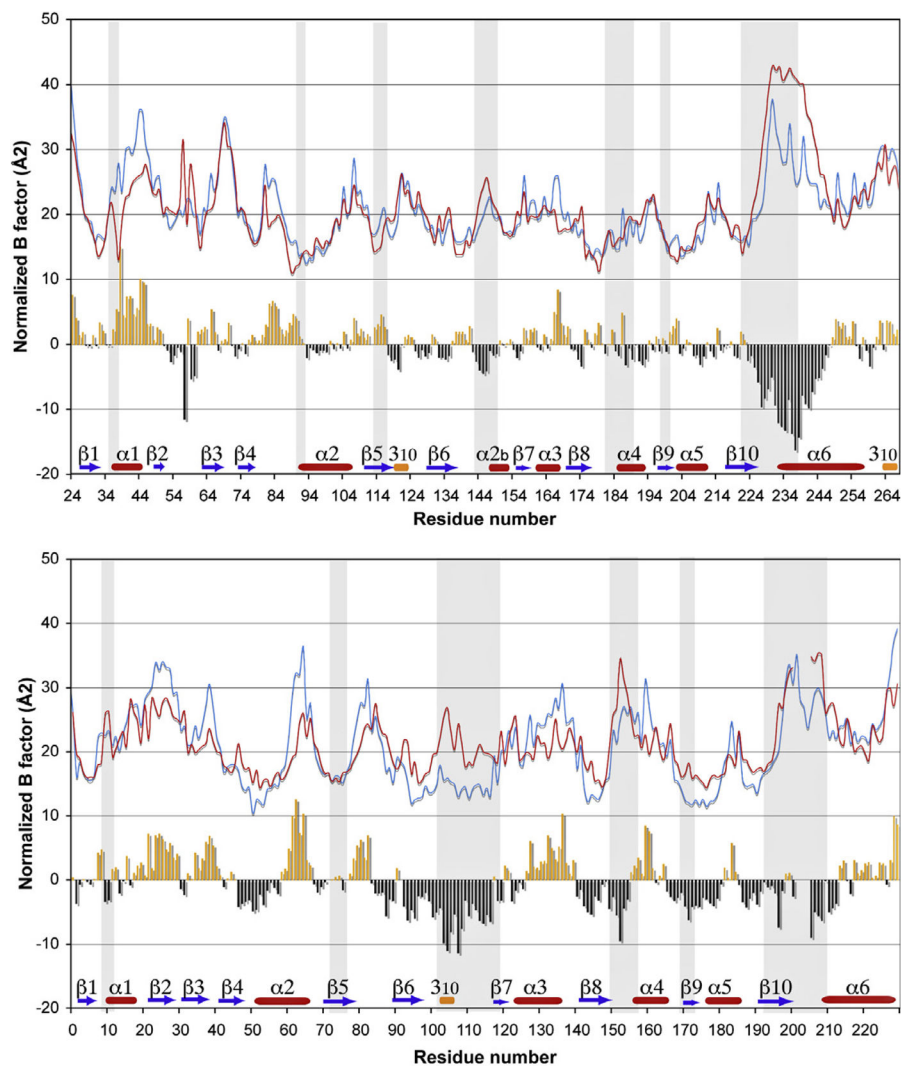


Fig. 5. B factor comparison of *Aa*MTAN1 and *Ec*MTAN. The differences in B factors between the open and closed states of (a) *Aa*MTAN1 and (b) *Ec*MTAN. The B factors of all structures were standardized to the average B factor of all protein atoms in *Aa*MTAN1-MTT (PDB: 2Q7G). B factors of the open and closed states are plotted in red and blue, respectively. Regions highlighted in grey indicate residues that are involved in substrate binding. The differences in B factors between the open and closed states are presented in the bar graph, where orange and black indicate an increase and decrease in B factors upon the binding of a ligand, respectively. The topologies of the enzymes are illustrated above the residue numbers. Please note that B factor information is not available for residues 202–205 in *Ec*MTAN-ADE (PDB: 1JYS). (For interpretation of the references to colour in this figure legend, the reader is referred to the web version of this article.)

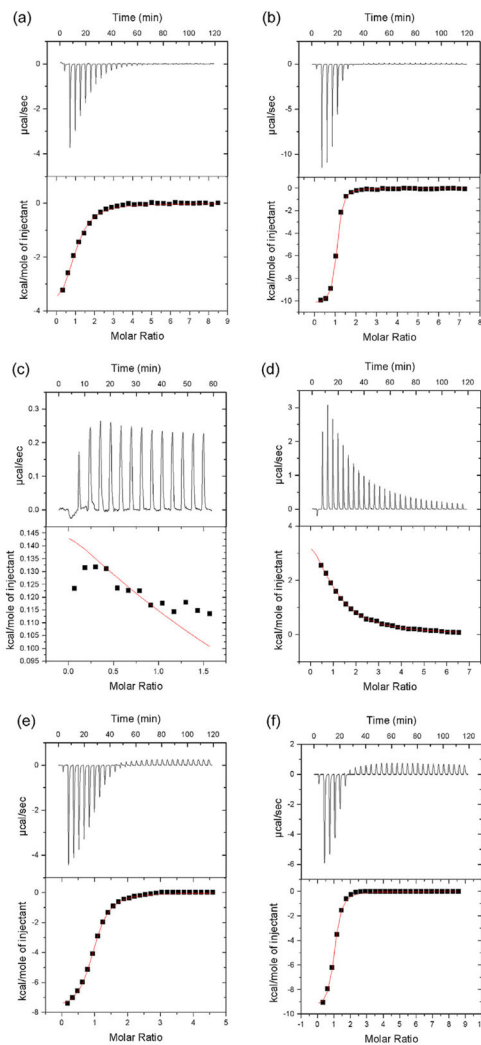


Fig. 6. Binding of SAH, MTA and ADE to *At*MTAN1 and *Ec*MTAN1. The binding isotherms for the titrations of (a) *At*MTAN1 with SAH, (b) *At*MTAN1 with ADE, (c) *At*MTAN1-E202Q with SAH, (d) *At*MTAN1-E202Q with MTA, (e) *Ec*MTAN1-E174Q with SAH and (f) *Ec*MTAN1-E174Q with MTA. No interaction is detected between *At*MTAN1-Glu202Gln and SAH. The top panel shows the changes in heat over time as the ligand is titrated into the protein solution. The bottom panel shows the normalized change in heat after subtracting reference data of ligand injections into buffer. The single-binding site model was used to fit the binding isotherms and the fit is shown in red on the bottom panel.

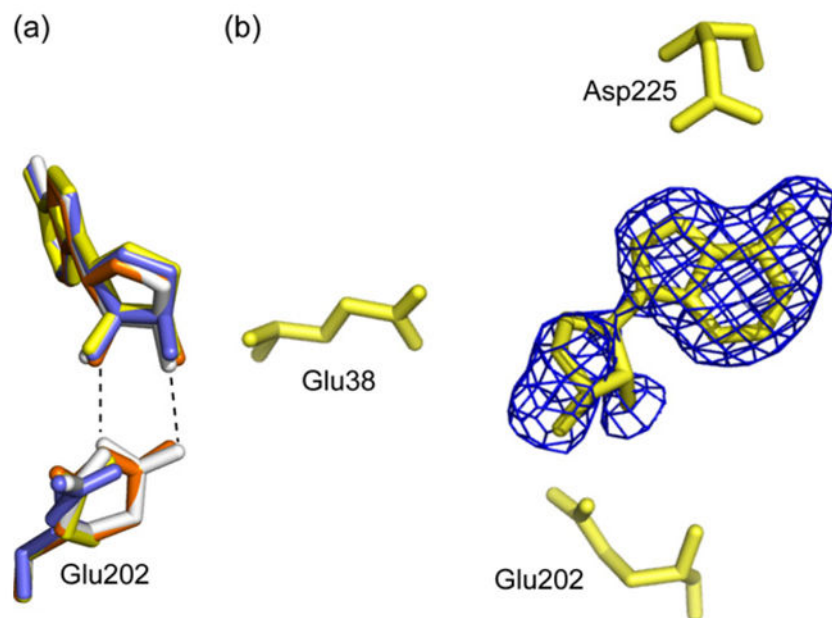


Fig. 7. The *AMTAN1*-SAH active site. (a) The catalytic residue, Glu202, is found in two conformations in the crystal structure of *AMTAN1* in complex with SAH. In monomers A and C, Glu202 is observed in the catalytic position at 40% occupancy. This orientation allows direct hydrogen-bond interactions with the substrate, which are essential for catalysis. The dominant conformation of Glu202 in all four monomers is too far for direct interaction with the ligand. Monomers A, B, C and D are illustrated in orange, yellow, white and blue, respectively. Hydrogen bonds are represented by dotted lines. (b) The experimental σ_A -weighted $3F_o - 2F_c$ electron density map, contoured at 0.8σ , superimposed over SAH in the refined structure. Adenine and SAH are each refined to 50% occupancy. The 5'-homocysteinyl substituent of SAH has not been modeled because no clear electron density was observed for this region. (For interpretation of the references to colour in this figure legend, the reader is referred to the web version of this article.)

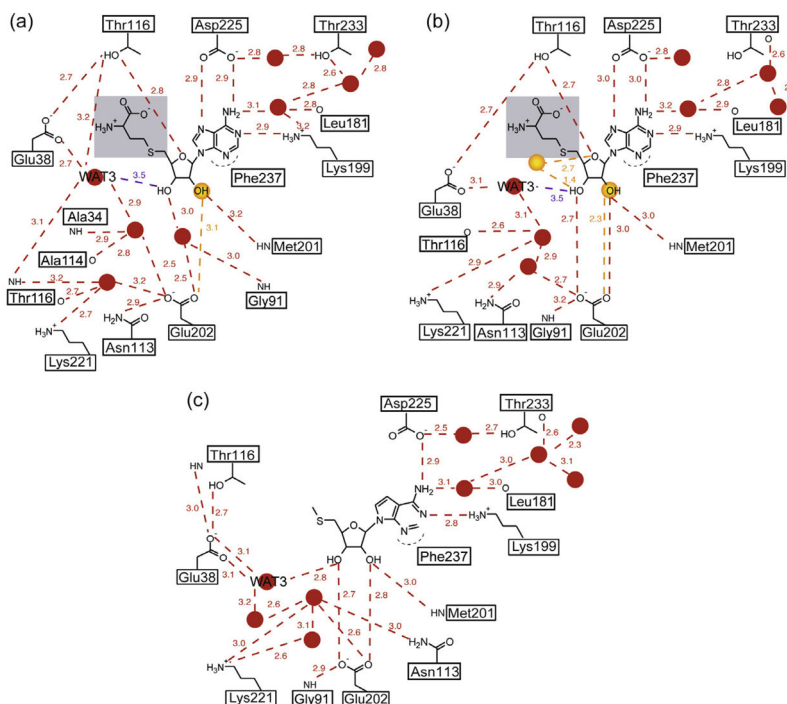


Fig. 8. Schematic representation of the ligand-bound *AMTAN1* active sites. Ligand interactions in (a) monomers B and D, and the dominant state of monomers A and C of *AMTAN1*-SAH, (b) the minor conformation of monomers A and C of *AMTAN1*-SAH, and (c) the structure of *AMTAN1* in complex with the substrate-analogue, MTT (PDB: 2QTG). Hydrogen bonds are represented by dotted lines. Distances are expressed in angstroms and correspond to the average distances observed in all monomers. The distance between WAT3 and SAH exceeds our definition of 2.2–3.2 Å for a hydrogen bond, and is represented in purple. Water molecules are represented by red circles. Water molecules that are present at half occupancy are coloured in orange. Panel (c) was adapted from Siu et al. (2008a).

Table 1

Thermodynamics for ligand binding to *A*MTAN1 and *Ec*MTAN.

Enzyme	Ligand	<i>A</i> MTAN1 SAH	<i>A</i> MTAN1 ADE	<i>A</i> MTAN1-E202Q SAH	<i>A</i> MTAN1-E202Q MTA	<i>A</i> MTAN1-E174Q SAH	<i>A</i> MTAN1-E174Q MTA	<i>Ec</i> MTAN-E174Q SAH	<i>Ec</i> MTAN-E174Q MTA
K_d (μ M)		24.8 \pm 2.6	1.7 \pm 0.1	Not detected	94.8 \pm 4.0	9.3 \pm 0.4	9.3 \pm 0.4	4.8 \pm 0.4	4.8 \pm 0.4
H (kcal/mol)		-4.4 \pm 0.2	-10.3 \pm 0.5		5.6 \pm 0.3	-7.9 \pm 0.1	-7.9 \pm 0.1	-9.6 \pm 0.1	-9.6 \pm 0.1
$-T \Delta S$ (kcal/mol)		-1.9	2.4		-11.1	1.0	1.0	2.4	2.4
N		0.99 \pm 0.03	0.99 \pm 0.003		0.97 \pm 0.04	0.94 \pm 0.01	0.94 \pm 0.01	0.94 \pm 0.01	0.94 \pm 0.01

Table 2

Data collection and refinement statistics.

A7MTAN1-SAH	
<i>Diffraction statistics</i>	
Space group	P2 ₁
Unit cell dimensions (Å)	
<i>a</i>	45.9
<i>b</i>	126.4
<i>c</i>	83.8
β (°)	101.7
No. observed reflections	173,922
No. unique reflections	46,037
Resolution range (Å)	23.12–2.20
<i>R</i> _{merge} (%) ^a	8.4 (28.9)
Redundancy	3.8
Completeness (%)	97.2 (95.2)
Average (<i>I</i> /σ <i>I</i>)	7.4 (3.0)
<i>Refinement statistics</i>	
No. of protein atoms	7524
No. of ligand atoms	68
No. of water molecules	519
Resolution range (Å)	23.12–2.20
No. reflections in test set	4627
Test set size (%)	10
<i>R</i> _{cryst} (%) ^b	20.8
<i>R</i> _{free} (%) ^c	26.2
Overall B factor (Å ²)	22.6
Ligands	20.0
Water	23.1
R.m.s. deviation	
Bonds (Å)	0.012
Angles (°)	1.4
Dihedral angles (°)	24.5
Improper angles (°)	3.0
Molprobrity output scores (%) ^e	
Ramachandran favored	98.1
Ramachandran outliers	0.0
Cruickshank's DPI based on <i>R</i> _{free} ^d	0.26

Values given in parentheses refer to reflections in the outer resolution shell: (2.28–2.20 Å).

^a $R_{\text{merge}} = \frac{\sum \sum |I(k) - \langle I \rangle|}{\sum I(k)}$, where $I(k)$ and $\langle I \rangle$ represent the diffraction intensity values of the individual measurements and the corresponding mean values. The summation is over all unique measurements.

$${}^b R_{\text{cryst}} = \frac{\sum ||F_{\text{obs}}| - k|F_{\text{calc}}||}{\sum |F_{\text{obs}}|}, \text{ where } F_{\text{obs}} \text{ and } F_{\text{calc}} \text{ are the observed and calculated structure factors, respectively.}$$

^c R_{free} is the sum extended over a subset of reflections (10%) excluded from all stages of the refinement.

^d Cruickshank's diffraction component precision index (DPI) as an estimate of coordinate error (Cruickshank, 1999).

^e As calculated using Molprobit (Lovell et al., 2003).